Self-Hybridized Vibrational-Mie Polaritons in Water Droplets

Adriana Canales, Oleg V. Kotov, Betül Küçüköz, and Timur O. Shegai[*]

Department of Physics, Chalmers University of Technology, 412 96 Göteborg, Sweden

We study the self-hybridization between Mie modes supported by water droplets with stretching and bending vibrations in water molecules. Droplets with radii > 2.7 μm are found to be polaritonic on the onset of the ultrastrong light-matter coupling regime. Similarly, the effect is observed in larger deuterated water droplets at lower frequencies. Our results indicate that polaritonic states are ubiquitous and occur in water droplets in mists, fogs, and clouds. This finding may have implications not only for polaritonic physics but also for aerosol and atmospheric sciences.

Water, one of the most widespread compounds on Earth, plays a vital role in a broad range of physical, chemical, biological, geological, atmospheric, and climate-related phenomena [1]. While being one of the most studied substances, water encompasses several unusual properties (e.g., triple point, anomalous density, anomalous heat expansion, etc.), some of which keep puzzling researchers [2,3]. Concurrently, advances in the realm of strong light-matter coupling have significantly impacted several research fields, including exciton transport [4–6], resonance energy transfer [7], photochemistry [8–10], charge transport [11], and ground-state chemical reactivity [12,13]. Central to these developments are polaritons— hybrid states of light and matter that arise as a result of strong coupling between photonic modes and a material's electronic or vibrational excitations [14]. Water is a promising polaritonic material platform, owing to its high oscillator strength, particularly in the midinfrared range [15]. Indeed, vibrational strong coupling between water and planar microcavities has been demonstrated in several works [16–22]. Self-assembled microcavities and polaritons have also been recently observed in aqueous solutions [23]. These realizations, however, required an external cavity, typically composed of two metallic mirrors.

To overcome the limitations of such cavities, *self-hybridized* polaritons have arisen recently. In these, optical modes supported by (nano)structured material's geometry hybridize with electronic or vibrational excitations of the same material [24]. These polaritons, inspired by Hopfield's work on bulk polaritons [25], have been studied in various systems, including excitonic slabs [26–30],

nanoparticle ensembles [31], nanodisks [32], nanotubes [33], and microspheres [34]. However, these observations were made in solid-state platforms. The potential existence of polaritons in liquids, and in water droplets in particular, has so far been shown only theoretically [24].

There are two fundamental advantages associated with studying polaritons within liquid droplets. First, the spherical geometry permits the exact solution of the electromagnetic eigenstate problem using Mie theory. Second, droplets form spontaneously, due to the liquid's high surface tension, resulting in nearly ideal spherical shapes. The latter renders water and oil droplets as promising whispering-gallery mode resonators, characterized by quality factors exceeding 10^7 [35,36], and as highly efficient Mie scatterers when subjected to optical levitation [37–39]. Moreover, a knowledge of electromagnetic eigenstates of water droplets is essential for an improved understanding of liquid water's properties. These eigenstates determine the spectroscopic characteristics of water droplets in the midinfrared range, which may impact scientific disciplines beyond polaritonics. These findings could, for instance, find implications in aerosol and atmospheric research, where previous measurements of water droplets in their clustered forms (e.g., mists, fogs, clouds) have shown spectroscopic peculiarities in the midinfrared range [40,41]. However, these peculiarities have not been previously interpreted in terms of vibrational-Mie self-hybridization.

Here, we study polaritonic eigenmodes of water droplets using Mie theory and infrared spectroscopy. We emphasize that one of the primary motivations behind this work is to characterize ensembles of polaritonic water droplets occurring naturally. For this reason, we measure the optical density of water droplet ensembles, comprising particles of various sizes, within a range of a few microns. To produce such a laboratory mist, we use a mesh nebulizer. The infrared spectroscopy data, in combination with Mie theory, reveals the polaritonic nature of the observed signal
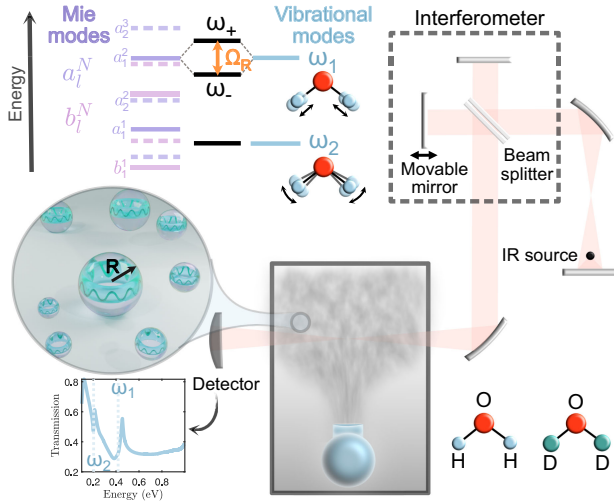
FIG. 1.   Concept of experiment on self-hybridized vibrational-Mie polaritons in water droplets. A vibrating mesh nebulizer generates a laboratory mist with droplet radii < 5 μm. Infrared spectroscopy in transmission (T) mode reveals Mie modes strongly coupled to molecular vibrations within water droplets, manifested in the emergence of polaritonic energy levels, $\hbar\omega_\pm$, separated by Rabi splitting, Ω_R. The experiments were performed with both regular (H_2O) and heavy (D_2O) water at different energy and droplet size ranges.

FIG. 2.   Polaritons in H_2O droplets. (a) Eigenfrequencies of $a_{l=1}^N$ as a function of droplet radius. In a certain size range, the mode splittings are observed. The Rabi splitting is marked with orange arrows. (b) The Rabi splitting increases with N and converges to the bulk Rabi splitting $2g_B$. (c) Calculated extinction cross sections of individual water droplets as a function of droplet size. The cross sections are calculated using experimental (Lorentz) permittivity shown in blue (dashed) lines. The uncoupled molecular vibrations are marked with vertical dotted lines. (d) Experimental and fitted optical density using the log-normal droplet size distribution shown in the inset. The gray dashed line shows calculated OD for the same size distribution but with vibrational modes artificially switched off, thus representing *uncoupled* spheres. Vertical dotted lines mark the position of regular water vibrations.

and the size distribution of droplets present in the samples. Furthermore, we conducted a similar experiment with deuterated (heavy) water and observed spectral shifts due to modified molecular vibrations and altered droplet sizes. These findings ensure that water droplets exhibit polaritonic self-hybridization between Mie modes of the spheres and molecular vibrations on the onset of ultrastrong light-matter coupling.

The laboratory mist used in the experiment was created using a vibrating mesh nebulizer (Evolu Air Pro) calibrated to produce droplets smaller than 5 μm radius with 0.9% saline water (Fig. S1 in the Supplemental Material [42]). As depicted in Fig. 1, the laboratory mist was set on the optical path of a Fourier transform infrared spectrometer (FTIR—Bruker Vertex 70v) in transmission (T) mode, covering the spectral range of 0.1 to 1 eV (1.2–12.4 μm). The optical density (OD) was then calculated as $OD = -\log(T)$. As we show below, the OD can be calculated via the extinction cross section of individual droplets using Beer-Lambert's law.

Water droplets forming the mist sustain Mie modes that interact with the symmetric and antisymmetric O-H stretching as well as the H-O-H bending vibrations. To demonstrate their polaritonic nature, we look for the main signature of strong coupling: the Rabi splitting (Ω_R) at zero detuning—the energy difference between upper ($\hbar\omega_+$) and lower ($\hbar\omega_-$) polariton branches (Fig. 1).

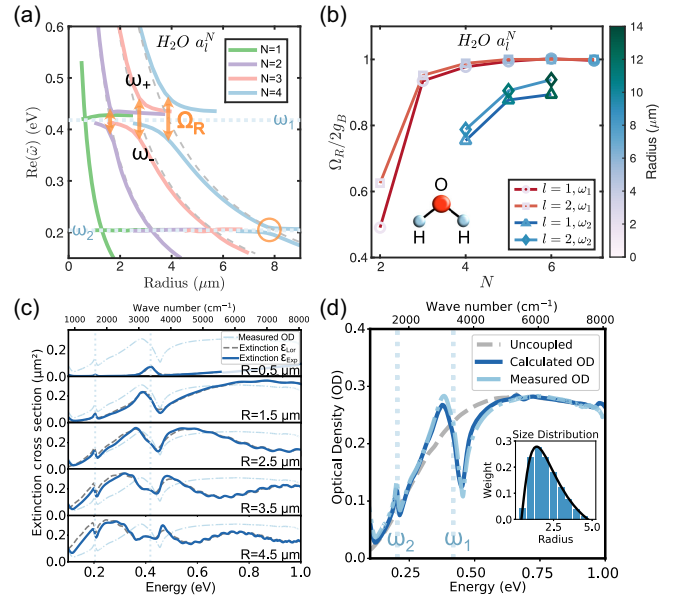Measuring the Rabi splitting in planar microcavities is straightforward because typically a spectrally isolated

optical mode(s) interacts with a single molecular vibration. In a mist containing droplets of various sizes, however, the OD aggregates the contributions of all Mie modes within individual droplets and accounts for the entire size distribution (Fig. 1), thus hindering direct observation of the Rabi splitting. Therefore, first, we calculate the modes resulting from the interaction between vibrations and single Mie modes in a sphere [Fig. 2(a)]. Then, the extinction spectrum of a single droplet with a fixed radius can be evaluated by summing all modes [Fig. 2(c)]. Finally, to account for specific size distribution, the extinction spectrum of the mist is obtained as a weighted sum of contributions from individual water droplets of varying diameters [Fig. 2(d)].

We start by calculating the eigenstates of individual water droplets. A water droplet is an open system; therefore we use complex eigenfrequencies to describe its quasinormal modes, $\tilde{\omega} = \omega - i\gamma/2$ [43]. The real part of the complex eigenfrequency describes the resonant frequency (ω), while the imaginary part describes its total decay rate, γ.

The eigenfrequencies are calculated as poles of the scattering coefficients given by the Mie solution [44]. Such scattering coefficients for a water sphere in air are

$$a_l = \frac{m\psi_l(mx)\psi_l'(x) - \psi_l(x)\psi_l'(mx)}{m\psi_l(mx)\xi_l'(x) - \xi_l(x)\psi_l'(mx)},$$

$$b_l = \frac{\psi_l(mx)\psi_l'(x) - m\psi_l(x)\psi_l'(mx)}{\psi_l(mx)\xi_l'(x) - m\xi_l(x)\psi_l'(mx)}. \quad (1)$$

Here, the size parameter, $x = kR$, includes light's wave vector k and the radius of the droplet, R. We use the Ricatti-Bessel functions $\psi_l(x) = x j_l(x)$ and $\xi_l(x) = x h_l^{(1)}(x)$, where $j_l(x)$ are spherical Bessel functions of the first kind, and $h_l^{(1)}(x)$ are Hankel functions of the first kind. The relative refractive index $m = n_{\text{water}}/n_{\text{air}}$, where $n_{\text{air}} = 1$ and $n_{\text{water}} = \sqrt{\varepsilon(\omega)}$, with $\varepsilon(\omega)$ being the water permittivity.

To analytically calculate the complex eigenfrequencies, the experimental water permittivity [45] was approximated by a Lorentzian function, $\varepsilon(\omega)$, using the fitting provided by Fiedler *et al.* [15] for the infrared region of interest (0.1–1 eV):

$$\varepsilon(\omega) = \varepsilon_\infty + \frac{f_1\omega_1^2}{\omega_1^2 - \omega^2 - i\gamma_1\omega} + \frac{f_2\omega_2^2}{\omega_2^2 - \omega^2 - i\gamma_2\omega}, \quad (2)$$

where $\varepsilon_\infty = 1.75$ accounts for all higher energy excitations. Because of their spectral overlap, we model the symmetric and antisymmetric O-H stretching as one effective oscillator with $\omega_1 = 0.418$ eV, a high oscillator strength $f_1 = 0.0717$, and a decay rate $\gamma_1 = 0.0341$ eV [46]. The H-O-H bending was considered as one oscillator with $\omega_2 = 0.204$ eV, an oscillator strength of $f_2 = 0.0134$, and decay rate of $\gamma_2 = 0.0084$ eV [15].

The scattering coefficients in Eq. (1) are associated with two types of modes: transverse magnetic (TM) and transverse electric (TE). TM (TE) eigenfrequencies are found when the denominator of the scattering coefficients a_l (b_l) equals zero. The multipole mode number l represents the number of electromagnetic field maxima around the circumference of the droplet. For a fixed angular number l and radius R, multiple mode orders occur at different energies with varying radial numbers, N. This mode order specifies the maxima in the radial direction inside the droplet [37]. To specify the mode in the text, we write a_l^N and b_l^N, which is equivalent to TM_{lN} and TE_{lN} [34,39].

These modes coexist within a water droplet and contribute to its extinction cross section. For a given radius, the extinction cross section reads

$$\sigma_{\text{ext}} = \frac{2\pi}{k^2} \sum_{l=1}^{\infty} (2l + 1)\mathfrak{Re}(a_l + b_l), \quad (3)$$

which we evaluate numerically using MiePython [47].

We use Beer-Lambert's law to represent the OD as a sum of extinction cross sections for each radius R_i, weighted by their concentrations n_i, $OD = L\sum_i n_i(R_i)\sigma_{\text{ext}_i}(R_i)$ [41]. Here, L is the optical path length through the mist. Then, we fit the experimental OD using the total normalized extinction cross section with the weight coefficients $w_i(R_i, L) \sim L n_i(R_i)$:

$$OD = \sum_i w_i(R_i, L)\sigma_{\text{ext}_i}(R_i). \quad (4)$$

The weights and radii in the size distribution were optimized to fit the experimental OD, using the log-normal distribution of mist from mesh nebulizers, as indicated by previous reports [48–50], and the experimental water permittivity [15]. The range of droplet radii produced by the mesh nebulizer was obtained from Evolu (Fig. S1 in the Supplemental Material). Fitting attempts with other radii ranges were unsuccessful (Fig. S7 in the Supplemental Material).

We start by analyzing a_1^N for different radii in Fig. 2(a). The real part of the eigenfrequencies is shown with colored lines for the first four radial numbers. The first radial mode (green) is weakly coupled to both water vibrations since the modes cross at zero detuning. The points of zero detuning occur where the uncoupled Mie modes (gray dashed lines) cross with the uncoupled H_2O vibrational modes (blue dotted lines). Droplets with radii below 1.5 μm only support the lowest TM and TE modes, resulting in weak coupling for all such droplets. See Fig. S2 in the Supplemental Material for the eigenfrequencies of other modes.

However, larger droplets can support higher N modes, resulting in mode splitting with ω_1 for $N \geq 2$ and ω_2 for $N \geq 4$ [Fig. 2(a)]. The Rabi splitting is marked with orange arrows. The onset of strong coupling is found when $\Omega_R > \gamma_{\text{avg}} = [(\gamma_M + \gamma_v)/2]$ [51]. Therefore, despite the visible splitting with ω_2 for $N = 4$ circled in Fig. 2(a), it is only strongly coupled after $N = 6$ (Fig. S4 in the Supplemental Material). On the other hand, the splitting with ω_1 is enough to be strongly coupled for $N \geq 3$, which corresponds to water droplets with radii above 2.7 μm.

Figure 2(a) displays an increase in Rabi splitting with higher N due to the decay rate of the Mie mode getting closer to the vibrational mode, visible in the complex frequency plane (Fig. S3). This results in a reduced $\delta\gamma = \gamma_M - \gamma_v$, which increases the Rabi splitting since $\Omega_R = 2\sqrt{g^2 - (\delta\gamma/4)^2}$. The same pattern occurs for higher l [Fig. 2(b)].

Despite the observed increase of the Rabi splitting for higher-order modes, it eventually saturates [Fig. 2(b)], with the ultimate limit set by the bulk Rabi splitting [24,34], $2g_B = \omega_1\sqrt{f/\varepsilon_\infty} \approx 85$ meV. Interestingly, Fig. S6 in the Supplemental Material shows that $\Omega_R/2\omega \approx 0.1$, meaning that the system has reached the onset of the ultrastrong

coupling (USC) regime for which $g/\omega \approx \Omega_R/2\omega > 0.1$ [52–54]. These results agree with previous studies of USC in water [17,21].

For a fixed radius, all hybridized modes contribute to light scattering and absorption, collectively yielding a water droplet's extinction cross section described by Eq. (3). The smallest droplets investigated in Fig. 2(c) are weakly coupled, as evidenced by mode crossing. On the other hand, while the largest radius has many hybridized modes, the Rabi splitting is not directly visible in the extinction spectra shown in Fig. 2(c). This is caused by many different hybridized and nonhybridized modes with different detunings contributing to the total extinction cross section. For the same reason, although there are two clear peaks in the spectra for a 2.5 μm droplet, it is incorrect to interpret it as Rabi splitting.

The mist is formed by a large number of droplets of various radii. Thus, none of the single-radius spectra matches the experimental OD [light blue dot-dashed line in Fig. 2(c)]. To calculate the OD and find the droplet size distribution, we used Eq. (4). To minimize any potential discrepancies stemming from the Lorentzian approximation (gray dashed lines), we employed the experimental permittivity of water (solid blue line) in our fitting, particularly noticeable in the largest radii in Fig. 2(c). The calculated OD that best fits the experiment is shown in Fig. 2(d), along with the log-normal droplet size distribution. A gray dashed line shows the extinction spectrum calculated for the same size distribution but with the oscillator strength of the vibrational modes artificially set to zero (i.e., uncoupled droplets). As for the case of individual droplets, it is important to note that despite the presence of two peaks in Fig. 2(d), care should be taken not to interpret the energy difference between them as Rabi splitting. Instead, the Rabi splitting is quantified individually for each Mie mode [Fig. 2(a)], whereas the two peaks observed in OD result from a complex combination of hybridized and nonhybridized modes across numerous droplets of varying sizes.

To ensure that the observed spectral features for regular water arise from optical and vibrational mode hybridization, we conducted a similar experiment and analysis with heavy water (D$_2$O, 99.9% Sigma-Aldrich). Although heavy water shares similar optical properties with regular water, its vibrational modes are shifted to lower frequencies due to the increased mass of deuterium in comparison to protium. This red shift corresponds to a factor of $\approx\sqrt{2}$. Hence, we expect that in heavy water droplets, the Rabi splitting appears at different energies and for different droplet sizes.

In this case, the Lorentzian permittivity was fitted to the experimental values [55]. The O-D stretch was set to $\omega_{1_{D_2O}} = 0.31$ eV, with the same oscillator strength as regular water [56] $f_{1_{D_2O}} = 0.0717$, but with smaller decay rate [57] $\gamma_{1_{D_2O}} = 0.0307$ eV in Eq. (2). Similarly, the D-O-D bending was set to $\omega_{2_{D_2O}} = 0.15$ eV, with the
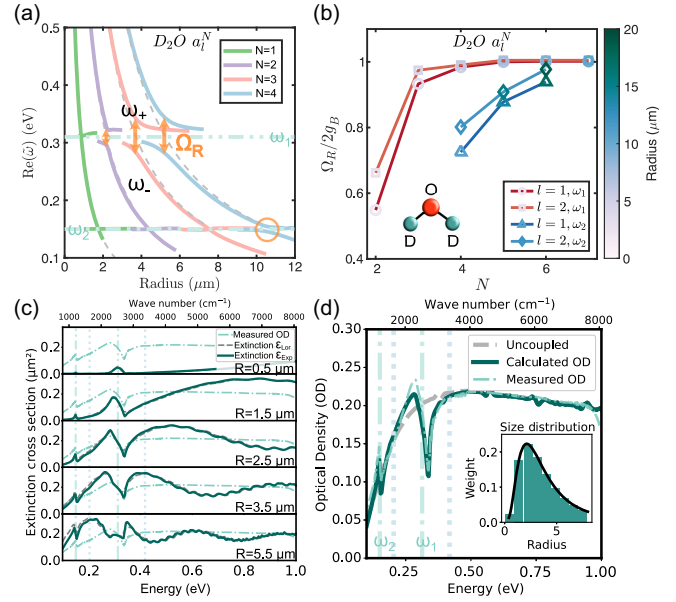

FIG. 3. Polaritons in D$_2$O droplets. (a) Eigenfrequencies of $a^N_{l=1}$ as a function of droplet radius. In a certain size range, the mode splittings are observed. The Rabi splitting is marked with orange arrows. (b) The Rabi splitting increases with N and converges to the bulk Rabi splitting $2g_B$. (c) Calculated extinction cross sections of individual water droplets as a function of droplet size. The cross sections are calculated using experimental (Lorentz) permittivity shown in blue (dashed) lines. The uncoupled molecular vibrations of heavy (regular) water are marked with vertical dash-dotted (dotted) lines. (d) Experimental and fitted optical density using the log-normal droplet size distribution shown in the inset. The gray dashed line shows calculated OD for the same size distribution but with vibrational modes artificially switched off, thus representing *uncoupled* spheres. Vertical dash-dotted (dotted) lines mark the position of heavy (regular) water vibrations.

oscillator strength of $f_{2_{D_2O}} = 0.0134$ and decay rate of $\gamma_{2_{D_2O}} = 0.0076$ eV.

Like regular water, a^N_1 Mie modes exhibit mode splitting for $N \geq 2$ [Fig. 3(a)]. However, the Rabi splitting is large enough to enter the strong coupling regime only for $N \geq 3$ with radii exceeding ~3.7 μm (Fig. S5 in the Supplemental Material). Larger droplets are therefore necessary to reach strong coupling with heavy water.

Despite the larger radii required for strong coupling, the Rabi splitting for heavy water droplets increases for larger N, similar to regular water. Figure 3(b) shows that the Rabi splitting increases until it saturates to the level of bulk Rabi splitting, which in the case of $\omega_{1_{D_2O}}$ is $2g_B \approx 63$ meV. Heavy water also reaches the onset of USC (Fig. S6 in the Supplemental Material).

After accounting for the contributions of all modes, we obtain the extinction cross sections for heavy water droplets of various radii [Fig. 3(c)]. We observe that the size of the droplet plays a crucial role in determining whether the

system enters the strong coupling regime. As for the case of regular water, the two clear peaks observed for $R = 2.5$ μm cannot be used as a measure of Rabi splitting.

It is important to note that the size distribution of heavy water droplets deviates from that of regular water droplets, owing to variations in physical properties such as ion concentration and viscosity [58]. The inset of Fig. 3(d) displays the size distribution that fits the OD of the heavy water droplets, produced in the same way and conditions as regular water droplets. We observe a larger mean droplet size in the distribution of heavy water compared to regular water. Unsuccessful attempts to fit OD with alternative size distributions are shown in Fig. S8 in the Supplemental Material. Of note is that our experimental data agree well with the fits obtained using the log-normal distributions of water droplet sizes for both regular and heavy water cases [see insets in Figs. 2(d) and 3(d), respectively].

This experiment shows that switching regular water to its heavy analog results in a spectrally shifted Rabi splitting because the vibrational modes of heavy water are red-shifted. Moreover, in this case, larger droplets with radii exceeding 3.7 μm demonstrate strong coupling. This size requirement is notably greater than the minimal size for regular water droplets, which is 2.7 μm.

The size limit necessary to reach the polaritonic regime in (heavy) water droplets implies that only about half of the droplets are strongly coupled in our laboratory mists. In nature, different types of fogs, mists, and clouds exhibit distinct size distributions of droplets. For example, a typical marine cloud's mean size is well into the polaritonic regime [59,60]. At the same time, droplets in a fog can be below the polaritonic limit [61].

To conclude, we employed infrared spectroscopy and Mie theory to measure and analyze the optical density of laboratory mists generated using a mesh nebulizer. We found that the spectra arise from the scattering and absorption of multiple Mie modes, which are strongly coupled to the vibrations of water molecules. We showed that there is a minimal size limit for polaritons to occur. Regular (heavy) water droplets with radii exceeding ∼2.7 μm (∼3.7 μm) are found to be polaritonic and can even reach the ultrastrong coupling regime. These water droplet sizes are naturally present in mists, fogs, and clouds [40,59,62]. The polaritonic eigenstates found in these water droplets raise questions about the impact of strong light-matter coupling on their spectroscopic and material properties. Aerosol, atmospheric, and climate researchers may be interested in studying this impact, particularly through monitoring the droplets' size, the interaction of different aerosols, and the admixture of dissolved molecules to water droplets. Finally, we foresee that droplet polaritons could be realized in nonaqueous liquids.

The data supporting the findings of this study are available within the Letter and its Supplemental Material [42].

*Corresponding author: timurs@chalmers.se

[1] F. H. Stillinger, Science **209,** 451 (1980).

[2] K. H. Kim, K. Amann-Winkel, N. Giovambattista, A. Späh, F. Perakis, H. Pathak, M. L. Parada, C. Yang, D. Mariedahl, T. Eklund et al., Science **370,** 978 (2020).

[3] J. Yang, R. Dettori, J. P. F. Nunes, N. H. List, E. Biasin, M. Centurion, Z. Chen, A. A. Cordones, D. P. Deponte, T. F. Heinz et al., Nature (London) **596,** 531 (2021).

[4] J. Feist and F. J. Garcia-Vidal, Phys. Rev. Lett. **114,** 196402 (2015).

[5] J. Schachenmayer, C. Genes, E. Tignone, and G. Pupillo, Phys. Rev. Lett. **114,** 196403 (2015).

[6] M. Balasubrahmaniyam, A. Simkhovich, A. Golombek, G. Sandik, G. Ankonina, and T. Schwartz, Nat. Mater. **22,** 338 (2023).

[7] D. M. Coles, N. Somaschi, P. Michetti, C. Clark, P. G. Lagoudakis, P. G. Savvidis, and D. G. Lidzey, Nat. Mater. **13,** 712 (2014).

[8] J. A. Hutchison, T. Schwartz, C. Genet, E. Devaux, and T. W. Ebbesen, Angew. Chem. Int. Ed. **51,** 1592 (2012).

[9] B. Munkhbat, M. Wersäll, D. G. Baranov, T. J. Antosiewicz, and T. Shegai, Sci. Adv. **4,** eaas9552 (2018).

[10] V. N. Peters, S. Prayakarao, S. R. Koutsares, C. E. Bonner, and M. A. Noginov, ACS Photonics **6,** 3039 (2019).

[11] E. Orgiu, J. George, J. Hutchison, E. Devaux, J. Dayen, B. Doudin, F. Stellacci, C. Genet, J. Schachenmayer, C. Genes et al., Nat. Mater. **14,** 1123 (2015).

[12] A. Thomas, L. Lethuillier-Karl, K. Nagarajan, R. M. Vergauwe, J. George, T. Chervy, A. Shalabney, E. Devaux, C. Genet, J. Moran et al., Science **363,** 615 (2019).

[13] W. Ahn, J. F. Triana, F. Recabal, F. Herrera, and B. S. Simpkins, Science **380,** 1165 (2023).

[14] F. J. Garcia-Vidal, C. Ciuti, and T. W. Ebbesen, Science **373,** eabd0336 (2021).

[15] J. Fiedler, M. Boström, C. Persson, I. Brevik, R. W. Corkery, S. Y. Buhmann, and D. F. Parsons, J. Phys. Chem. B **124,** 3103 (2020).

[16] R. M. Vergauwe, A. Thomas, K. Nagarajan, A. Shalabney, J. George, T. Chervy, M. Seidel, E. Devaux, V. Torbeev, and T. W. Ebbesen, Angew. Chem. Int. Ed. **58,** 15324 (2019).

[17] T. E. Li, J. E. Subotnik, and A. Nitzan, Proc. Natl. Acad. Sci. U.S.A. **117,** 18324 (2020).

[18] J. Lather and J. George, J. Phys. Chem. Lett. **12,** 379 (2020).

[19] K. Hirai, H. Ishikawa, T. Chervy, J. A. Hutchison, and H. Uji-i, Chem. Sci. **12,** 11986 (2021).

[20] M. V. Imperatore, J. B. Asbury, and N. C. Giebink, J. Chem. Phys. **154,** 191103 (2021).

[21] T. Fukushima, S. Yoshimitsu, and K. Murakoshi, J. Phys. Chem. C **125,** 25832 (2021).

[22] T. Fukushima, S. Yoshimitsu, and K. Murakoshi, J. Am. Chem. Soc. **144**, 12177 (2022).

[23] B. Munkhbat, A. Canales, B. Küçüköz, D. G. Baranov, and T. O. Shegai, Nature (London) **597**, 214 (2021).

[24] A. Canales, D. G. Baranov, T. J. Antosiewicz, and T. Shegai, J. Chem. Phys. **154**, 024701 (2021).

[25] J. Hopfield, Phys. Rev. **112**, 1555 (1958).

[26] B. Munkhbat, D. G. Baranov, M. Stührenberg, M. Wersäll, A. Bisht, and T. Shegai, ACS Photonics **6**, 139 (2018).

[27] R. Gogna, L. Zhang, and H. Deng, ACS Photonics **7**, 3328 (2020).

[28] P. A. Thomas, K. S. Menghrajani, and W. L. Barnes, J. Phys. Chem. Lett. **12**, 6914 (2021).

[29] A. Canales, O. Kotov, and T. Shegai, ACS Nano **17**, 3401 (2023).

[30] F. Dirnberger, J. Quan, R. Bushati, G. M. Diederich, M. Florian, J. Klein, K. Mosina, Z. Sofer, X. Xu, A. Kamra et al., Nature (London) **620**, 533 (2023).

[31] N. S. Mueller, Y. Okamura, B. G. Vieira, S. Juergensen, H. Lange, E. B. Barros, F. Schulz, and S. Reich, Nature (London) **583**, 780 (2020).

[32] R. Verre, D. G. Baranov, B. Munkhbat, J. Cuadra, M. Käll, and T. Shegai, Nat. Nanotechnol. **14**, 679 (2019).

[33] R. Pandya, R. Chen, Q. Gu, J. Sung, C. Schnedermann, O. S. Ojambati, R. Chikkaraddy, J. Gorman, G. Jacucci, O. D. Onelli et al., Nat. Commun. **12**, 6519 (2021).

[34] C. E. Platts, M. A. Kaliteevski, S. Brand, R. A. Abram, I. V. Iorsh, and A. V. Kavokin, Phys. Rev. B **79**, 245322 (2009).

[35] S. Maayani, L. L. Martin, and T. Carmon, Nat. Commun. **7**, 10435 (2016).

[36] A. Giorgini, S. Avino, P. Malara, P. De Natale, and G. Gagliardi, Sci. Rep. **7**, 41997 (2017).

[37] A. D. Ward, M. Zhang, and O. Hunt, Opt. Express **16**, 16390 (2008).

[38] J. Kher-Alden, S. Maayani, L. L. Martin, M. Douvidzon, L. Deych, and T. Carmon, Phys. Rev. X **10**, 031049 (2020).

[39] J. T. Marmolejo, A. Canales, D. Hanstorp, and R. Méndez-Fragoso, Phys. Rev. Lett. **130**, 043804 (2023).

[40] H. H. Blau, R. P. Espinola, and E. C. Reifenstein, Appl. Opt. **5**, 555 (1966).

[41] W. P. Arnott, C. Schmitt, Y. W. Liu, and J. Hallett, Appl. Opt. **36**, 5205 (1997).

[42] See Supplemental Material at http://link.aps.org/supplemental/10.1103/PhysRevLett.132.193804 for additional experimental and theoretical details.

[43] P. Lalanne, W. Yan, K. Vynck, C. Sauvan, and J. P. Hugonin, Laser Photonics Rev. **12**, 1 (2018).

[44] C. F. Bohren and D. R. Huffman, *Absorption and Scattering of Light by Small Particles* (Wiley, New York, 2004), p. 530.

[45] D. J. Segelstein, The complex refractive index of water, Ph. D. thesis, University of Missouri–Kansas City, 1981.

[46] B. Bagchi, Dynamics of water: Molecular motions and hydrogen-bond-breaking kinetics, in *Water in Biological and Chemical Processes: From Structure and Dynamics to Function, Cambridge Molecular Science* (Cambridge University Press, Cambridge, England, 2013), pp. 27–60.

[47] S. Prahl, *MiePython: Pure python implementation of Mie scattering* (2023), 10.5281/zenodo.8218010.

[48] K. McDermott and J. G. Oakley, Curr. Ther. Res. **94**, 100623 (2021).

[49] P. Sharma, M. Quazi, I. R. Vazquez, and N. Jackson, J. Aerosol Sci. **166**, 106072 (2022).

[50] S. Niazi, L. K. Philp, K. Spann, and G. R. Johnson, Appl. Environ. Microbiol. **87**, e00497 (2021).

[51] P. Törmä and W. L. Barnes, Rep. Prog. Phys. **78**, 013901 (2014).

[52] C. Ciuti, G. Bastard, and I. Carusotto, Phys. Rev. B **72**, 115303 (2005).

[53] A. Frisk Kockum, A. Miranowicz, S. De Liberato, S. Savasta, and F. Nori, Nat. Rev. Phys. **1**, 19 (2019).

[54] P. Forn-Díaz, L. Lamata, E. Rico, J. Kono, and E. Solano, Rev. Mod. Phys. **91**, 025005 (2019).

[55] J.-J. Max and C. Chapados, J. Chem. Phys. **131**, 184505 (2009).

[56] M. Pastorczak, K. Duk, S. Shahab, and A. A. Kananenka, J. Phys. Chem. B **127**, 4843 (2023).

[57] L. De Marco, W. Carpenter, H. Liu, R. Biswas, J. M. Bowman, and A. Tokmakoff, J. Phys. Chem. Lett. **7**, 1769 (2016).

[58] T. Ghazanfari, A. M. Elhissi, Z. Ding, and K. M. Taylor, Int. J. Pharm. **339**, 103 (2007).

[59] N. L. Miles, J. Verlinde, and E. E. Clothiaux, J. Atmos. Sci. **57**, 295 (2000).

[60] C. Zhao, L. Zhao, and X. Dong, Atmosphere-Ocean **10**, 19 (2019).

[61] S. S. Muhammad, B. Flecker, E. Leitgeb, and M. Gebhart, Opt. Eng. (Bellingham, Wash.) **46**, 066001 (2007).

[62] Y. Benayahu, A. Ben-David, S. Fastig, and A. Cohen, Appl. Opt. **34**, 1569 (1995).